ELSEVIER

Journal of Magnetism and Magnetic Materials 145 (1995) 57–66

journal of magnetism and magnetic materials

Mössbauer spectroscopy of Cr(110)/Fe(110)/Cr(110) sandwiches

J. Zukrowski [1], G. Liu, H. Fritzsche, U. Gradmann *

Physikalisches Institut, Technische Universität Clausthal, D 38678 Clausthal–Zellerfeld, Germany

Received 10 June 1994; in revised form 3 October 1994

Abstract

Magnetic order in ultrathin Fe(110) films in a Cr(110) matrix and its temperature dependence were analyzed using conversion electron Mössbauer spectroscopy (CEMS). The samples were characterized by flat interfaces, as tested by SPA-LEED (spot profile analysis LEED). Fe films consisting of D atomic layers with $1 \leq D \leq 31$ were doped by ^{57}Fe probes and analyzed using CEMS in situ in UHV, for 100 K $\leq T \leq$ 450 K. All spectra could be fitted by Zeeman sextets with $B_{hf}(T)$ following Bloch laws. For films with $2 \leq D \leq 6$, the first Fe layer in the CrFe interface shows a reduced ground state hyperfine field of $B_s(0) = 25.8$ T, which differs from values determined previously for rough interfaces. It agrees roughly with the predictions from an alloy model. Spin-wave parameters are reduced in comparison with samples W(110)/Fe/Ag. For thicker films ($D > 6$), two subcomponents of the interface can be distinguished, with equal abundance, but different hyperfine fields and different b parameters; apparently they belong to two magnetically inequivalent states resulting from the antiferromagnetic order in Cr. Extraordinary low values for the surface enhancement of the b parameters, $\alpha_{s,a} = 1.5$ and $\alpha_{s,b} = 1.1$, respectively, and a large value of 10 atomic distances for the interaction length are explained by the antiferromagnetic order of the matrix. The low values for the surface enhancement of the spin-wave parameters differ strongly from results reported for the case of rough interfaces. For the double layer, a break of $B_{hf}(T)$ was observed near the Néel temperature of Cr. Parameters of the monolayer could be roughly determined.

1. Introduction

One of the basic problems in thin film magnetism is the local structure of thermal decrease of magnetic order. How does this thermal decrease change from atomic layer to atomic layer in an ultrathin film? The problem is typical of the spin-wave regime well below T_c; it does not apply in the critical regime, where as a result of the long-wavelength character of the critical fluctuations magnetic order becomes homogeneous along the surface normal. The problem has been addressed in theory by molecular field [1, 2], Monte Carlo [3] and Green's functions [4] methods. A tight relation to the problem of enhanced thermal decrease near the surfaces of thick samples [3,5,6] is obvious. In experiment, ^{57}Fe Mössbauer spectroscopy offers the unique chance to experimentally check the problem for the case of Fe based films. The high local resolution required can be achieved if ^{57}Fe probe layers are embedded in a film consisting otherwise of ^{56}Fe, resulting in a local measurement of the magnetic hyperfine field B_{hf} in

* Corresponding author. Fax: +49-5323-72-3600; Email: grad mann@physik.tu-clausthal.de.

[1] Permanent address: Department of Solid State Physics FPNT, Academy of Mining and Metallurgy, 30-059 Cracow, Poland.

SSDI 0304-8853(94)00408-J

the probe-layer position. The method was pioneered by Tyson et al. [7], who used transmission Mössbauer spectroscopy and probes consisting of a few atomic layers to analyze Fe(110) films on Ag(111). The use of true monolayer ^{57}Fe probes and thus true monolayer resolution was achieved by introducing Conversion Electron Mössbauer Spectroscopy (CEMS) in situ in UHV [8–10]. Extended application has been made to Fe(110) films on W(110) with different coverages [11–15], down to the thermodynamically stable monolayer Fe(110) on W(110) [16–19]. It turned out that B_{hf} can be used as a measure for the thermal decrease of the magnetization and its local variation, but not for the magnitude of the magnetization. For a review see Ref. [20].

For a quantitative discussion of the thermal decrease of B_{hf}, a description by a Bloch law,

$$B_{hf}(T) = B_{hf}(0)[1 - bT^{3/2}], \quad (1)$$

turns out to provide a good approximation in a surprisingly wide range of conditions, even down to the monolayer [16], where a theoretical foundation is missing. The advantage of this description is that one single parameter only, given by this Bloch (spin-wave) parameter b, is needed as a measure of thermal decrease. The local structure of the thermal decrease of magnetization then reduces to the local profile of b. This convenient description of thermal decreasing magnetization for temperatures well below T_c using b parameters is now widely used in the literature, and so we use it in what follows. In addition to the work on Fe(110) on W(110), CEMS probe layer analysis of Fe/Cr(100,110) interfaces [21–23] and monolayer probe CEMS analysis of Fe(100)/W(100) and Fe(100)/Ag interfaces [24] has been performed based on this approach. Typically, b is enhanced in the first Fe layer of an interface, in comparison with bulk Fe, by a factor between 2 and 3, with an exponential transition from the surface to the bulk value in a regime given by an 'interaction length' of typically 2 to 3 atomic layer distances.

In the present study, we extend the previous work on Fe(110) on W(110) [16–19] to Fe(110) on Cr(110). This is interesting for several reasons. Firstly, it seems interesting to compare these related systems with respect to the thermal decrease of ferromagnetic order. The in-plane symmetry is the same in both systems. However, there is a clear difference in the misfit to the substrate, which is comparatively large (9.4%) on W, but extremely small (0.7%) on Cr. In addition, the previous films on W(110) were embedded in a nonmagnetic matrix (W, Ag, UHV), in contrast to the present films, which are embedded in an antiferromagnetic Cr matrix. How does the b parameter profile react to this changed surroundings? Secondly, there is considerable interest in the Cr/Fe epitaxial system in connection with indirect coupling, which actually was detected first for Fe(100)/Cr(100)/Fe(100) sandwiches [25] and investigated in great detail for this orientation [26–28], which now can be considered as one of the best-known systems of indirect coupling. In remarkable contrast, there exists to our knowledge only one short note [29] on indirect coupling in Fe(110)/Cr(110)/Fe(110). This absence of published data on coupling by Cr(110) may be connected with a considerable tendency for kinetic roughening [30] or facetting [31] in the autoepitaxial and the heteroepitaxial growth of bcc(110) films. Accordingly, coupling phenomena might be hidden to a considerable extent for typical preparations at room temperature. It will be shown that rather smooth Cr(110) films can be prepared on W(110) at elevated temperatures (560 K). This provides an opportunity to perform the present CEMS study of ultrathin Fe(110) films on Cr(110) starting with smooth Cr substrates; the study then provides a useful contribution to the epitaxial preparation of Cr/Fe(110) sandwiches and multilayers in general. It will be shown that our results fit well with the related investigation of bulk-like Cr/Fe(110) interfaces of Landes and coworkers [21–23], with characteristic differences which can be explained from a substantial reduction of interface roughness in our samples in comparison with those of Landes and coworkers.

We discuss our experimental conditions in section 2, preparation and structure of the films in section 3, present the CEMS data in section 4 and discuss the results in section 5.

2. Experimental conditions

The main experiments were done in a CEMS spectrometer described previously [10]. Sandwiches consisting of ^{57}Fe, ^{56}Fe and Cr were prepared by

MBE on atomically smooth and clean W(110) surfaces, at pressures below 10^{-10} Torr. Film thickness could be controlled for each component separately with an absolute accuracy of 5% of a monolayer. Film thickness is given in units of bulk Fe(110) monolayer equivalents, D. Because of the small misfit $f_{CrFe} = -0.7\%$, D equals the true number of monolayers within the limits of accuracy. Film structure could be tested in the CEMS system by standard LEED and by AES using a CMA. CEMS analysis was done using grazing incidence of γ-quanta from a moving single line CoRh source of initially 100 mCi. Conversion electrons were counted using a channeltron, to which the sample was imaged in an energy filtering mode using a spherical condenser. The spectrum of one monolayer ^{57}Fe could be obtained typically in one day. Sample temperatures could be varied between 90 and 2000 K. They were measured using a WRe thermocouple.

More detailed analysis of the growth conditions, in particular on the surface roughness induced by kinetic roughening and facetting, was done in a separate UHV system, equipped with a high sensitivity torsion oscillation magnetometer (TOM), and in particular with a commercial SPA-LEED (spot profile analysis LEED) system for high angular resolution analysis of the LEED spots. The transfer width of the system (largest distance of resolvable steps) is of the order of 100 nm. The system was used in our previous studies on kinetic facetting in Fe(110) on W(110) [31], on magnetic step moments [32, 33] and on magnetic step anisotropies [34] in Fe(110) surfaces.

3. Preparation and structure of the films

The preparation of atomically clean and flat Cr(110) substrates is difficult. In our case, they had to be prepared as secondary substrates, by epitaxial growth on W(110). Cr films of some 10 atomic layers, prepared at room temperature, showed a weak indication only of LEED spots, on a bright and nearly homogeneous background, pointing to a rather high density of structural imperfections, probably of volume type. With increasing temperatures, the intensity of the spots increased. Films prepared at 700 K showed sharp spots with the instrumental width

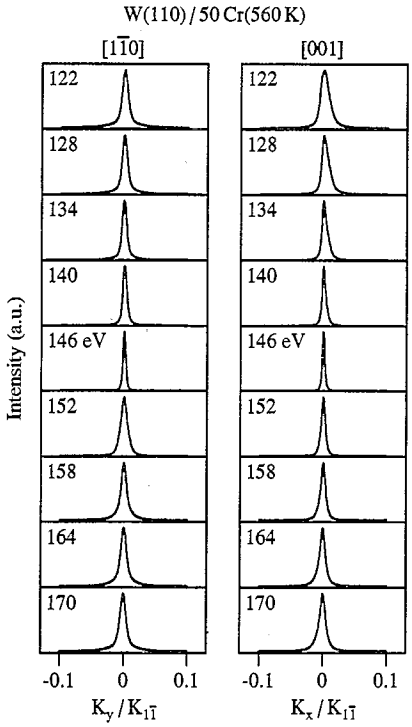

Fig. 1. Angular profiles of the specular LEED spot, taken in two orthogonal scans, along [1$\bar{1}$0] and [001], respectively, for 50 atomic layers of Cr, prepared at 560 K on W(110). Electron energies are given as parameters; the in-phase energy is near 146 eV.

only; however, even for 50 ML Cr, the AES signal of the W substrate became visible for preparation or after annealing at 700 K. Apparently, the microscopic surfaces became flat at these high preparation temperatures only at the expense of the film breaking up into Stranski–Krastanov like crystallites. For the present study, we had to compromise, that means to prepare at temperatures low enough to avoid islanding and high enough to provide reasonable flatness. We prepared our Cr(110) substrates, consisting of roughly 40 ML, at 560 K. The surface was characterized by the angular structure of the specular LEED spot, observed by SPA-LEED, as shown in Fig. 1 for a sample W(110)/50Cr(560 K) (i.e. 50 atomic layers of Cr, prepared at 560 K) in two orthogonal scans along [1$\bar{1}$0] and [001], respectively, for different electron energies given as parameters. As indicated by the orthogonal scans, the spots were approximately circular. Accordingly, the surface step structures are two-dimensional, opposite to the case of

Fe(110) on W(110), where ridge-like step systems along [001] only have been observed [31]. For the in-phase energies of 146 eV, where the spot profile is insensitive to atomic steps, we observe a widening of the spot profiles to roughly 0.3% of the first Brillouin zone, in comparison with the instrumental width of 0.1%. This indicates a minor level of volume type defects. An energy-dependent broadening of the spots to about 0.8% at 122 eV, near the out-of-phase energy, indicates an irregular step structure with step distances of the order of 100 atomic distances. Note that the width of all spot profiles in Fig. 1 is below the instrumental width of standard LEED systems; optical inspection in standard LEED equipment would result in the statement of 'excellent LEED spots'. The step structure being two-dimensional, we roughly estimate the contribution of step atoms to be of the order of 2%.

The following Fe films, consisting of D atomic layers, were prepared at 300 K in order to completely avoid any Cr/Fe interdiffusion; they were coated finally at 300 K by Cr, resulting in samples of type W(110)/40Cr(560 K)/DFe(300 K)/Cr(300 K). For the structure of the Fe films, we relied on a related SPA-LEED study of films prepared on thinner Cr substrates, W(110)/12Cr(560 K)/DFe(300 K) [30]. In those films we observed the same type of one-dimensional kinetic facetting which was observed before for the auto-epitaxy of Fe(110) on Fe(110) [31], with ridges along [001]. The mean

Table 1
Parameters of samples W(110)/40Cr(560 K)/$\underline{D}_1 + D_2 + \underline{D}_3$ (300 K)/Cr(300 K) consisting of two or more Fe layers ($\underline{D}_1 + D_2 + \underline{D}_3 \geq 2$); the columns contain the current number of the sample, the type of the sample (in short notation), the component in question, its ground state hyperfine field $B_{hf}(0)$, its spin-wave parameter b, and its relative contribution in the CEMS spectrum, R, both from experiment and theory, respectively

Nr.	Type	Layer	$B_{hf}(0)$ (T)	b ($\times 10^{-6}$ K$^{-3/2}$)	R (%)		
					Exp.		Theor.
1	Cr/2.0/Cr	s ($T < T_N$)	25.3(1)	16.0(5)	86		100
		s ($T > T_N$)	26.3(1)	23.4(4)			
		c	34.1(2)	13.1(7)	14		0
2	Cr/3.3/Cr	s	25.8(1)	13.1(3)	57		61
		s − 1	34.5(1)	12.2(4)	43		39
3	Cr/4.0/Cr	s	25.8(1)	12.7(4)	48		50
		s − 1	34.8(1)	11.3(5)	52		50
4	Cr/6.0/Cr	s	25.8(1)	11.7(6)	34		33.3
		s − 1	36.0(1)	11.2(4)	33		33.3
		s − 2	34.0(1)	9.0(3)	33		33.3
5	Cr/3 + 4 + 3/Cr	s_a	25.6(2)	9.9(7)	15	32	33.3
		s_b	29.5(2)	5.7(8)	17		
		s − 1	35.6(1)	9.7(1)	34		33.3
		s − 2	34.2(1)	8.5(4)	34		33.3
6	Cr/3 + 4 + 3/Cr	c	34.2(1)	6.8(1)			
7	Cr/3 + 25 + 3/Cr	s_a	25.3(2)	8.4(4)	18	32	33.3
		s_b	29.1(2)	6.3(5)	14		
		s − 1	35.3(1)	8.0(3)	34		33.3
		s − 2	34.1(1)	7.9(3)	34		33.3
8	Cr/3 + 2 + 21 + 2 + 3/Cr	s − 3	34.7(1)	7.4(2)			
		s − 4					
9	Cr/13 + 5 + 13/Cr	c	34.2(1)	5.7(1)			
10	bulk Fe		34.1	5.3			

width of atomic levels, given by the number N of atomic chains between two steps, is proportional to $D^{-1/2}$ for Fe grown both on Fe(110) and Cr(110). Surprisingly, the step distance is larger for Fe(110) on Cr(110) $[N = 52D^{-1/2}]$ than for Fe(110) on Fe(110) $[N = 23D^{-1/2}]$. We expect that these structural issues apply roughly to the present films, too. Summarizing, we conclude that the contribution of step atoms is hardly more than a fraction of 10% of the surface atoms, and step atoms therefore can be neglected in the present approach.

4. Mössbauer results

The present study is based on 13 samples with a total Fe thickness between $D = 1$ and $D = 31$ monolayers. 8 samples contained pure ^{57}Fe components. Indicating ^{57}Fe components by underlining ($\underline{D}$), we characterize these pure ^{57}Fe samples by W(110)/30Cr(560 K)/$\underline{D}$Fe(300 K)/Cr(300 K), short notation Cr/$\underline{D}$/Cr. 5 additional samples contained ^{57}Fe probes only, e.g. Cr/$\underline{3}$ + 4 + $\underline{3}$/Cr with symmetric ^{57}Fe probes consisting of 3 atomic layers each (underlined). For a first group of 9 samples with a total Fe thickness $D \geq 2$, CEMS spectra were taken for an extended series of temperatures between 90 and 400 K. For a second group of 4 samples in the monolayer regime, spectra were measured only at 90 and 300 K. We discuss the two groups separately, starting with the thicker Fe films.

4.1. Samples containing two or more Fe layers

A compilation of all films with a total number of Fe layers $D \geq 2$ is given in Table 1. Typical spectra are shown in Fig. 2a, hyperfine fields versus temperature in Fig. 2b, fitted by Bloch laws. We dispense with a presentation of isomer shifts and quadrupole splittings, which actually contain only information of minor importance. For sample 1, {Cr/$\underline{2}$/Cr}, two different Bloch law branches had to be used for $T > 300$ K and $T < 300$ K, respectively; these are documented separately in Fig. 3 by plotting B_{hf} versus $T^{3/2}$. A graphical representation of all Bloch b parameters across the different components of the samples is given in Fig. 4.

We comment the fitting procedure as follows:

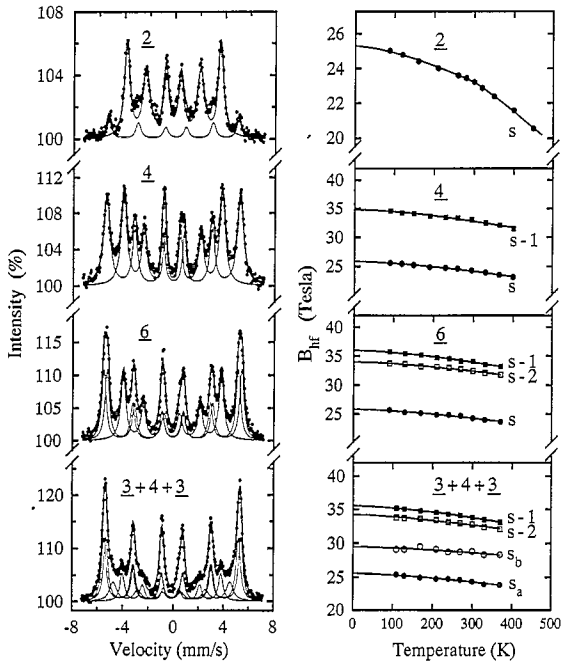

Fig. 2. CEMS analysis of samples containing two or more Fe layers. Most samples are of type W(110)/40Cr(560 K)/$\underline{D}$/^{57}Fe(300 K)/Cr(300 K), containing $\underline{D}$ atomic layers of pure ^{57}Fe only (short notation $\underline{D}$ included in the figures). One thicker sample Cr/$\underline{3}$+4+$\underline{3}$/Cr contains a sequence of 3 layers ^{57}Fe, 4 layers ^{56}Fe and further 3 layers ^{57}Fe, respectively. (a) (left panel): CEMS spectra, taken at 300 K, component decomposition indicated. (b) (right panel): Hyperfine fields B_{hf} versus temperature for surface layer component s, subcomponents s_a and s_b of the first surface layer, and for first and second subsurface layer components s-1 and s-2, respectively.

(a) The pure ^{57}Fe samples {Cr/$\underline{D}$/Cr} with $2 \leq \underline{D} \leq 6$ (samples 1–4) were fitted in a straightforward manner with 2 or 3 components (surface layers, first and second subsurface layers s-1 and s-2, and central

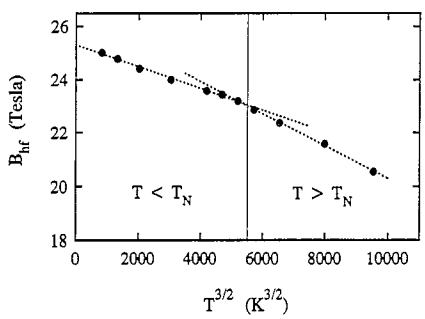

Fig. 3. Hyperfine field B_{hf} versus $T^{3/2}$, for a double layer Cr/$\underline{2}$/Cr (first sample in Fig. 2). The Néel temperature of bulk Cr (313 K) is indicated by the vertical line.

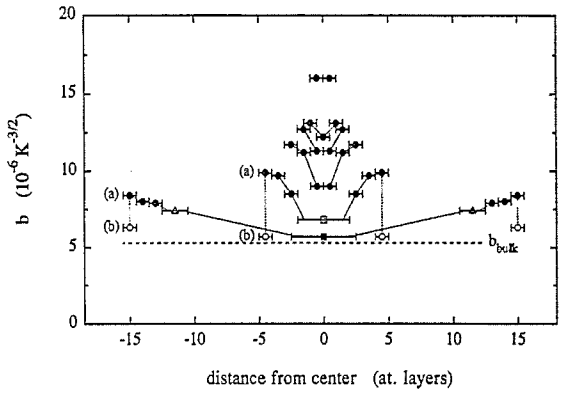

Fig. 4. Spin-wave parameters versus distance from the film center, for the samples of Table 1. Two subcomponents (a) and (b) of the interface layer are given by filled and open circles, respectively.

layer c) as suggested by an ideal structural model. This fitting is justified by the excellent agreement between experimental and theoretical values of the relative contributions R, and by the constant value of the ground state field $B_s(0) = 25.8$ T of the surface component. These findings indicate a quite good approximation to layer-by-layer growth. The assessment of components s-1 and s-2 in sample 4 {Cr/6/Cr} is consistent with the monotonic decrease of the b parameter, and with the enhancement of $B_{s\text{-}1}(0)$ as detected previously by Sauer et al. [23]. For the double layer only a discontinuity was observed near the Néel temperature of the Cr matrix at 307 K.

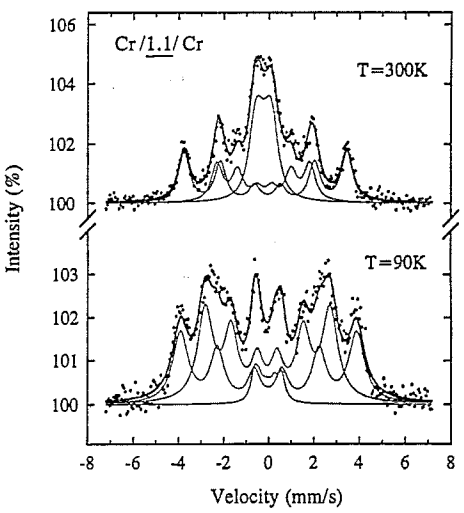

Fig. 5. CEMS spectra, taken at 300 and 90 K, respectively, for a sample Cr/1.1/Cr.

(b) For the samples with ^{57}Fe surface probes containing 3 atomic layers, sample 5, {Cr/3 + 4 + 3/Cr} and sample 7, {Cr/3 + 25 + 3/Cr}, we first tried a 3 components fit, as suggested by the number of probe layers. This turned out to be inadequate both with respect to the fitting quality and to the relative contributions, the surface component with $B_s(0) = 25.8$ T having a quite unreasonable $R_s = 20\%$ only. It turned out that for both samples the spectra could be conveniently fitted only with 4 components, including two sub-components s_a and s_b of the surface layer, with a reasonable total surface $R_s = 32\%$. As mean values from both samples, we obtain $B_{s,a}(0) = (25.4 \pm 0.2)$ T, $B_{s,b}(0) = (29.3 \pm 0.2)$ T, $b_{s,a} = (9 \pm 1) \times 10^{-6}$ $K^{-3/2}$ and $b_{s,b} = (6 \pm 1) \times 10^{-6}$ $K^{-3/2}$, respectively. A surprising finding is the quite low value of $b_{s,b}$, which is very near to the bulk value. A tentative interpretation will be given in the last section.

(c) For the samples 6, 8, 9 with inner probes, a single component fit was used.

4.2. Films near the monolayer

In addition to the thicker films of the last section, four samples Cr/D/Cr in the monolayer regime were evaluated, with $D = 0.80$, 1.00, 1.04 and 1.10, respectively. Only spectra at 90 and 300 K were measured for these samples. The mode of evaluation is shown for the example $D = 1.10$, the spectra of which are shown in Fig. 5. They were fitted at both temperatures by 3 components; relative contributions and magnetic hyperfine fields are collected in Table 2 for the components 1,2 and 3, at 90 and 300 K, respectively. The magnitude of $B_2(90\text{ K}) = 24.3$ T, in comparison with sample 1 from Table 1, strongly suggests that component 2 is indeed a double layer

Table 2
Relative contributions R and hyperfine fields B_{hf} for the spectra of sample Cr/1.1/Cr given in Fig. 5

T (K)	Component	R (%)	B (T)
	1	44	17.2
90	2	47	24.3
	3	9	3.8
	1	28	12.8
300	2	27	22.5
	3	35	2.8

component. It is then reasonable to use the two values $B_2(90\ \mathrm{K})$ and $B_2(300\ \mathrm{K})$ to determine $B_2(0) = 24.6$ T and $b_2 = 16.6 \times 10^{-6}\ \mathrm{K}^{-3/2}$. The fair agreement with sample 1 from Table 1 confirms the attribution and the mode of evaluation. We then guess that component 1 is the monolayer component, and roughly determine $B_1(0) = 18.1$ T and $b_1 = 56 \times 10^{-6}\ \mathrm{K}^{-3/2}$ as monolayer parameters. With respect to component 3, note that its relative contribution rapidly increases, with increasing temperature, from 9% at 90 K to 35% at 300 K. We suppose that it is something like a component consisting of small patches, monolayer or double layers, which become superparamagnetic with increasing temperatures. It seems then reasonable to roughly assume that component 3 would disappear at 0 K at the expense of both other components. It is then further reasonable to assume that $R_2(90\ \mathrm{K})/R_1(90\ \mathrm{K})$ gives the ratio of atoms in the double layer and monolayer patches, respectively. If the coverage by double layers, monolayers and free surface are given by θ_2, θ_1 and θ_0, respectively, with $\theta_0 + \theta_1 + \theta_2 = 1$, one finally arrives at model values of the θ_n. Coverages determined in this approximation are shown in Fig. 6 for the 4 samples of the monolayer series. Their dependence on D is reasonable: Whereas θ_2 increases monotonically with increasing D, and θ_0 decreases monotonically, θ_1 reaches its maximum at $D = 1$. Apparently, complete layer-by-layer growth does not take place in the initial stage, but monolayer patches are dominant at $D = 1$. By collecting the data of the 4 samples, we determined mean values for the Bloch law parameters, resulting in $B_1(0) = (19.6 \pm 1.2)$ T, $b_1 = (61.4 \pm 6) \times 10^{-6}\ \mathrm{K}^{-3/2}$, $B_2(0) = (24.7 \pm 0.4)$ T and $b_2 = (17.6 \pm 0.3) \times 10^{-6}\ \mathrm{K}^{-3/2}$. The good agreement of the latter parameters with those of the true double-layer sample 1 in Table 1 confirms that these parameters are real monolayer and double layer properties, respectively.

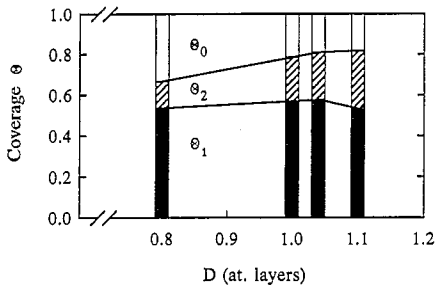

Fig. 6. Coverages θ_0, θ_1 and θ_2 of Fe-free areas, monolayer and double layer patches, respectively, in pure ^{57}Fe films Cr/$\underline{D}$/Cr, in the monolayer regime.

5. Discussion

5.1. Film structure

The very good agreement of the experimentally determined relative contributions for $D \geq 2$ with the theoretical expectations from a layer growth model, as seen in Table 1, confirms that a layer-by-layer growth mode is realized to a very good approximation, for the present preparation of very thin single films at $T_p = 560$ K. This is in accordance with the SPA-LEED profiles published previously [30]. It applies for $D \geq 2$, and if the components s_a and s_b are interpreted as subcomponents of one common surface layer component; the interpretation of which will be discussed below. It should be emphasized, however, that our previous work on kinetic roughening and facetting in bcc(110) films [30,31] shows that both a reduction of preparation temperature or an increase of the total thickness of the epitaxial sample would result in a substantial increase of the surface roughness, in accordance with recent analysis of epitaxial growth of Fe on Fe(001) [35].

Contrary to the case of Fe(110) on W(110), where the pseudomorphic monolayer is thermodynamically stable and therefore can be prepared with a high degree of perfection [19], it was impossible to prepare a perfect monolayer of Fe(110) on Cr(110); some admixture of double-layer patches could not be avoided, see Fig. 6. This might surprise at first glance, because the misfit of Fe is small with respect to a Cr substrate ($f_{\mathrm{FeCr}} = -0.7\%$) and large to a W substrate ($f_{\mathrm{FeW}} = -9.4\%$). Correctly interpreted, however, this illustrates the frequently neglected fact that the stability of a heteroepitaxial monolayer, and the possibility to prepare it, is a matter of surface energies of the substrate (high for the high melting W substrate) rather than of the lattice misfit [20].

5.2. Magnetic hyperfine fields

We interprete the magnetic hyperfine fields in the surface and for the monolayer in comparison with

Cr–Fe alloys as investigated by Dubiel and Zukrowski [36], who showed that for a wide range of Cr–Fe alloys the magnitude of B_{hf} at a Fe atom is determined by the numbers Z_1 and Z_2 of nearest and next-nearest Cr neighbours. The reduction of B_{hf} in comparison with its bulk value is given, according to their alloy analysis, by

$$\Delta B_{hf} = -(3.19Z_1 + 2.17Z_2). \quad (2)$$

Applying this alloy model to surface atoms, we use $Z_1 = Z_2 = 2$, resulting in $\Delta B_s = -10.7$ T. Experimentally, $B_s(0) = 25.8$ T is a common value of samples 2,3 and 4 in Table 1. Comparison with the bulk value in line 10 results in an experimental value of $\Delta B_s = -8.3$ T, in rough agreement with the predictions from the alloy model. For the monolayer, we use $Z_1 = Z_2 = 4$, to predict $\Delta B_s = 21.4$ T from the alloy model, in fair agreement with the experimental value $\Delta B_s = -17.4$ T, which is again a bit smaller than the predicted one. Note that the experimental reduction for the monolayer is twice the reduction for the surface, just as expected from the nearest neighbours counting.

Our experimental value $B_s(0) = 25.8$ T deviates from the value of 23.7 T reported by Sauer et al. [23]. We guess that the difference is connected with the interface roughness of their samples. Accordingly, we could not find any indication of the rich admixture of step components which Sauer et al. reported. For the subsurface layer, we obtain as a mean value from samples 3, 4, 5 and 7 of Table 1, $B_{s-1}(0) = (35.4 \pm 0.5)$ T, in fair agreement with 35.0 T as reported by Sauer et al. Note that $B_{s-2}(0) = (34.1 \pm 1)$ T again agrees with the bulk value. In other words, the oscillation of $B_{hf}(0)$ is restricted to the two outermost surface layers, consisting of a reduction in the first and an enhancement in the second one; this is similar to what was found previously for the free Fe(110) surface [9].

What is the meaning of the split surface component in samples 5 and 7 of Table 1? We note that both subcomponents s_a and s_b of the surface are of nearly equal abundance (as a mean value from both samples, we find $R_{s,a}/R_{s,b} = 1.06 \pm 0.2$). With respect to the comparatively flat interfaces of our samples, this is incompatible with an interpretation in terms of surface and step atoms. However, there is a magnetic asymmetry in this interface, which apparently has not been discussed so far. This asymmetry results from the antiferromagnetic order in the Cr matrix. Note that the easy axis of magnetization in the Fe(110) films in a Cr matrix is [001] as in bulk Fe, not [1$\bar{1}$0] as in the films on W(110). This is a result of different in-plane surface anisotropies in the W(110)/Fe(110) and the Cr(110/Fe(110) interfaces, respectively [37]. In antiferromagnetic Cr, the antiparallel sublattice magnetizations of (001) planes can be directed along $\pm$[001]. In the (110) interface, both antiparallel directions of Cr spins are present alternatingly for nearest neighbours Cr atoms, the plane being antiferromagnetically compensated. As a result, there are two magnetically inequivalent Cr positions in the interface with Fe(110), one with the Cr spin parallel to that of the nearest neighbour Fe atoms and one with the Cr spin antiparallel to them. It is reasonable that the hyperfine fields of the two positions differ by the 4 T found in experiment. This interpretation depends on antiferromagnetic order in Cr; it must therefore be assumed that magnetic order in Cr is induced in the interface by the Fe in contact with it. The absence of splitting for $D \leq 6$ could be explained by the assumption that, by unknown reasons, the Cr spins are directed along $\pm$[010], that means at right angles to the Fe spins; the asymmetry then would disappear. This interpretation is in accordance with the Bloch parameters, to be discussed in the next subsection. However, it should be emphasized that an appropriate structural reconstruction as an alternative origin for the splitting of the surface component cannot be excluded. It remains to be discussed in how far part of the additional surface components reported by Sauer et al. [23] can be explained from the splitting observed in our flat interfaces.

5.3. *Thermal decrease of B_{hf} and spin-wave parameters*

It has been noted first by Rado [5] that the surface layer of a ferromagnet, like the volume, follows a spin-wave $T^{3/2}$ law (Eq. (1)), but with a surface Bloch parameter $b_s = \alpha_s\, b_{bulk}$ which is enhanced in comparison with the bulk value by a Rado enhancement factor α_s. For the case of a surface with negligible surface anisotropy, and with homogeneous exchange up to the surface, Rado predicted $\alpha_s = 2$

from a micromagnetic continuum model. This was confirmed by Mills and Maradudin [6] in a more sophisticated approach. Mathon [38] showed how a reduced exchange strength in the surface can result in a further enhancement above this Rado value, up to $\alpha_s > 2$. The transition from the surface type to the bulk type temperature dependence has been discussed in Monte Carlo simulations by Binder and Hohenberg [3]. Sauer et al. [23] noted that this transition can be phenomenologically described by an exponential profile for $\Delta b_i = b_i - b_{\text{bulk}}$, given by

$$\Delta b_{s-n} = \Delta b_s \exp(-n/\delta), \tag{3}$$

with an interaction length δ, and n being the distance of an atomic layer from the surface. Both parameters α_s and δ have been determined by CEMS for interfaces of Fe(110) with W(110) [11], Ag [9], UHV [9], Cr [23] and Gd [23]. A compilation given in Ref. [24], including Fe(100)/W(100) and Fe(100)/Ag interfaces, shows that the surface enhancement is always larger than the Rado prediction, $\alpha_s > 2$, and that δ typically ranges between 2 and 3.5.

For the present type of interface, Fe(110)/Cr(110), Sauer et al. [23] reported an exceedingly large surface enhancement of $\alpha_s = 3.6$, in combination with an exceedingly low value of $\delta = 0.7$. Our results for thick films ($D = 31$ in Fig. 4) are in sharp contrast. Even when using the larger value of subcomponent (a), we obtain $\alpha_s = 1.5$ only, definitely below Rado's value, and a rough estimate of $\delta = 10$. We suppose that the high value of α_s reported by Sauer et al. reflects the considerable roughness of their interfaces, and the high and reasonable sensitivity of α_s on it. Their low value of δ then is supposed to be an artifact produced by the high value of α_s. Apparently, our values are limiting values of the (nearly) flat interface. The most reasonable explanation for the exceedingly low value of α_s results from the antiferromagnetic order of the Cr matrix, which can be interpreted as a continuation of the magnetically ordered system; it is reasonable that α_s is lower in the interface with antiferromagnetically ordered substrates than with the nonmagnetic partners W, Ag or UHV. At the same time, the strong difference for surface components (a) and (b) becomes reasonable from the different coupling geometries.

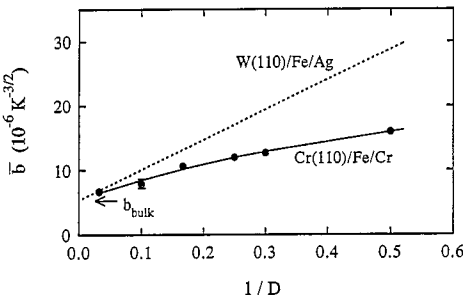

Fig. 7. Mean values $\bar{b}$ of the spin-wave parameter versus $1/D$ for samples Cr(110)/Fe/Cr containing D atomic layers of Fe(110). Results for W(110)/Fe/Ag (from Ref. [14]) for comparison.

In previous CEMS studies of Fe(110) films on W(110) covered with Ag (W(110)/Fe/Ag) [13], we observed two properties of spin-wave parameters b in ultrathin films: Firstly, the b parameters were independent on the position of the probe layer, for $D \leq 4$, as a result of the strong exchange coupling; in terms of spin waves, this results from the inability to excite modes with $k_z > 0$. Secondly, the mean value $\bar{b}$ showed a linear dependence on $1/D$ in general. The first observation is confirmed by the present study for Cr(110)/Fe/Cr, as seen from Fig. 4 and Table 1. The second issue is checked in Fig. 7, which shows a roughly linear dependence of b of $1/D$ for the present case too. However, $\bar{b}$ is definitely smaller for the films in the antiferromagnetic Cr matrix. This is a reasonable result of the stabilizing action of the magnetically ordered matrix on the ferromagnetic film.

As reported above in section 4.2, the Bloch parameter of the monolayer has an extremely high value of $b_1 = 56 \times 10^{-6}$ K$^{-3/2}$, very near to the value measured in the pseudomorphic monolayer on W(110), covered by Ag [13]. We can only speculate on the origin of this high value. The observation could be explained qualitatively by assuming an antiferromagnetic coupling between both Cr(110) half spaces, mediated by the intercalated Fe monolayer, which in turn would be softened in such a structure. A corresponding antiferromagnetic coupling between two Fe(110) films by an intercalating Cr(110) monolayer has been observed recently using KERR magnetometry [39].

Acknowledgements

This work was supported by the Deutsche Forschungsgemeinschaft. We thank J. Korecki and M. Przybylski for fruitful discussions and for critical reading of the manuscript.

References

[1] L. Valenta, Phys. Stat. Sol. 2 (1962) 112.
[2] Z. Onyszkiewicz and A. Wierzbicki, J. Magn. Magn. Mater. 99 (1991) 253.
[3] K. Binder and P.C. Hohenberg, Phys. Rev. B 9 (1974) 2194.
[4] W. Brodkorb and W. Haubenreisser, Phys. Stat. Sol. 16 (1966) 225, 577.
[5] G.T. Rado, Bull. Am. Phys. Soc. 112 (1957) 127.
[6] D.L. Mills and A.A. Maradudin, J. Phys. Chem. Solids 28 (1967) 1855.
[7] J. Tyson, A.H. Owens, J.C. Walker and G. Bayreuther, J. Appl. Phys. 52 (1981) 2487.
[8] J. Korecki and U. Gradmann, Phys. Rev. Lett. 55 (1985) 2491.
[9] J. Korecki and U. Gradmann, Europhys. Lett. 2 (1986) 651.
[10] J. Korecki and U. Gradmann, Hyperfine Interactions 28 (1986) 931.
[11] M. Przybylski, U. Gradmann and J. Korecki, J. Magn. Magn. Mater. 69 (1987) 199.
[12] M. Przybylski and U. Gradmann, Hyperfine Interactions 41 (1988) 693.
[13] M. Przybylski, I. Kaufmann and U. Gradmann, Phys. Rev. B 40 (1989) 8631.
[14] J. Korecki, M. Przybylski and U. Gradmann, J. Magn. Magn. Mater. 89 (1990) 325.
[15] M. Przybylski, J. Korecki and U. Gradmann, Hyperfine Interactions 57 (1990) 2053.
[16] M. Przybylski and U. Gradmann, Phys. Rev. Lett. 59 (1987) 1152.
[17] M. Przybylski and U. Gradmann, J. Appl. Phys. 63 (1988) 3652.
[18] M. Przybylski and U. Gradmann, J. de Phys. 49 (1988) C8.
[19] U. Gradmann, M. Przybylski, H.J. Elmers and G. Liu, Appl. Phys. A 49 (1989) 563.
[20] U. Gradmann, Magnetism in Ultrathin Transition Metal Films, in K.H.J. Buschow, Handbook of Magnetic Materials, Vol. 7/1 (Elsevier Science, Amsterdam, 1993) p. 1.
[21] J. Landes, C. Sauer, R.A. Brand, W. Zinn, S. Mantl and Z. Kajcsos, J. Magn. Magn. Mater. 86 (1990) 71.
[22] J. Landes, C. Sauer, R.A. Brand, W. Zinn and Zs. Kajcsos, Hyperfine Interactions 57 (1990) 1941.
[23] C. Sauer, J. Landes, W. Zinn and H. Ebert, Mater. Res. Soc. Symp. Proc. 231 (1992) 153.
[24] G. Liu and U. Gradmann, J. Magn. Magn. Mater. 118 (1993) 99.
[25] P. Grünberg, R. Schreiber, Y. Pang, M.B. Brodsky and H. Sowers, Phys. Rev. Lett. 57 (1986) 2442.
[26] J. Unguris, R.J. Celotta and D.T. Pierce, Phys. Rev. Lett. 67 (1991) 140.
[27] J. Unguris, R.J. Celotta and D.T. Pierce, Phys. Rev. Lett. 69 (1992) 1125.
[28] M. Rührig, R. Schäfer, A. Hubert, R. Mosler, J.A. Wolf, S. Demokritov and P. Grünberg, Phys. Stat. Sol (a) 125 (1991) 635.
[29] P. Grünberg, J. Barnas, F. Saurenbach, J.A. Fuss, A. Wolf and M. Vohl, J. Magn. Magn. Mater. 93 (1991) 58.
[30] H. Fritzsche and U. Gradmann, Mater. Res. Soc. Symp. Proc. 312 (1993) 321.
[31] M. Albrecht, H. Fritzsche and U. Gradmann, Surf. Sci. 294 (1993) 1.
[32] M. Albrecht, T. Furubayashi, U. Gradmann and W.A. Harrison, J. Magn. Magn. Mater. 104–107 (1992) 1699.
[33] M. Albrecht, U. Gradmann, T. Furubayashi and W.A. Harrison, Europhys. Lett. 20 (1992) 65.
[34] M. Albrecht, T. Furubayashi, M. Przybylski, J. Korecki and U. Gradmann, J. Magn. Magn. Mater. 113 (1992) 207.
[35] J.A. Stroscio, D.T. Pierce, R.A.J. Unguris, R.J. Celotta and R.A. Dragoset, Phys. Rev. Lett. 70 (1993) 3615.
[36] S.M. Dubiel and J. Zukrowski, J. Magn. Magn. Mater. 23 (1981) 214.
[37] H. Fritzsche, H.J. Elmers and U. Gradmann, J. Magn. Magn. Mater. 135 (1994) 343.
[38] J. Mathon, Physica B 149 (1988) 31.
[39] U. Gradmann, G. Liu and H.J. Elmers, to be published.